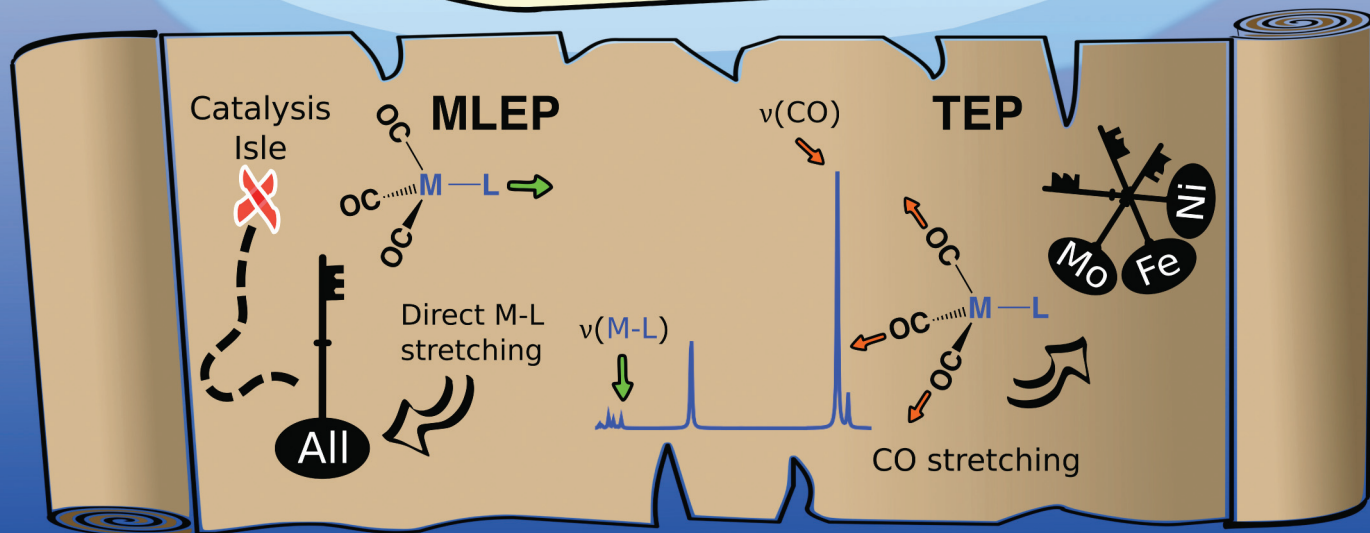
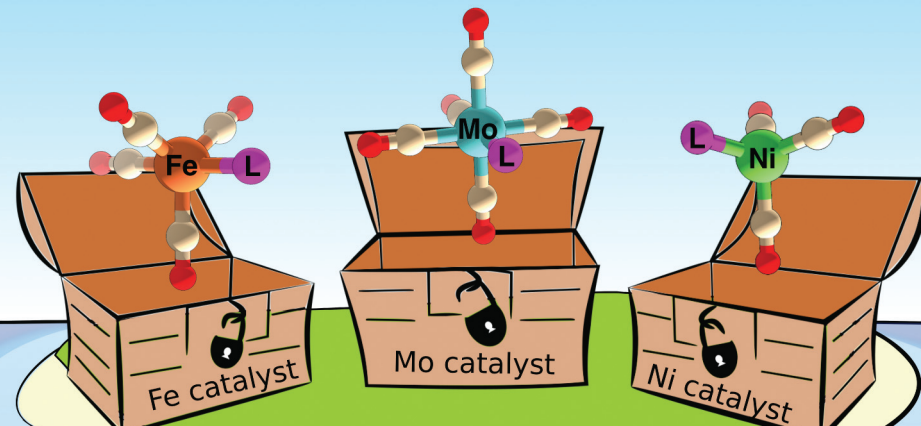


Dalton Transactions

An international journal of inorganic chemistry

rsc.li/dalton



ISSN 1477-9226



ROYAL SOCIETY
OF CHEMISTRY

PERSPECTIVE

Dieter Cremer and Elfi Kraka

Generalization of the Tolman electronic parameter: the metal–ligand electronic parameter and the intrinsic strength of the metal–ligand bond



Cite this: *Dalton Trans.*, 2017, **46**, 8323

Generalization of the Tolman electronic parameter: the metal–ligand electronic parameter and the intrinsic strength of the metal–ligand bond

Dieter Cremer* and Elfi Kraka

The catalytic activity of transition metal complexes $(R)_nM-L$ can be predicted utilizing the metal–ligand electronic parameter (MLEP) that is based on the local stretching force constant of the M–L bond. Vibrational spectroscopy is an excellent tool to accurately determine vibrational mode properties such as stretching frequencies. These correspond, because of mode–mode coupling, to delocalized vibrational modes, which have to be first converted into local vibrational modes, and their properties. Each bond of a molecule can be uniquely characterized by the local stretching force constant and frequency. The former is ideally suited to set up a scale of bond strength orders, which identifies weak M–L bonds with promising catalytic activity. It is shown how the MLEP replaces the TEP (Tolman Electronic Parameter), which is based on the CO stretching frequencies of a $(CO)_nM-L$ complex and which is now exclusively used in hundreds of investigations. However, the TEP is at best a qualitative parameter that suffers from relatively large mode–mode coupling errors and the basic deficiency of most indirect descriptors: They cannot correctly describe the intrinsic M–L bond strength *via* the CO stretching frequencies.

Received 16th January 2017,
Accepted 6th March 2017

DOI: 10.1039/c7dt00178a
rsc.li/dalton

1. Introduction

Some of the most widely used catalysts in homogeneous catalysis are transition metal complexes.^{1–11} For example, the annual Rhodium catalyzed production of aldehydes amounts to 10 million tons, 6 million of which lead to formaldehyde.^{12,13} There is a continuous scientific enterprise of finding new, even more efficient transition metal catalysts out of a huge number of possible combinations involving one of the 28 transition metals (M) of the first, second, and third transition metal period (excluding Tc) and a large number of possible ligands (L). Attempts to find suitable transition metal complexes for catalysis reach from trial-and-error procedures to educated guesses, model-based strategies, and quantum chemical descriptions of potential catalysts.^{1–7,10,14} In this connection, one has searched for parameters that can be simply measured and used as suitable descriptors to assess the catalytic activity of a transition metal complex. Clearly, electronic factors determining the metal–ligand interactions and thereby the availability of the metal for additional bonding play an important role. First attempts to describe the catalytic activity

of a transition metal complex in homogeneous catalysis focused on the determination of bond dissociation energies (BDEs)¹⁵ or molecular geometries to predict, *via* BDE values and/or bond lengths, the ease of replacement of a given ligand or the possibility of enlarging the coordination sphere of the transition metal during catalysis.

While these attempts have certainly benefited the chemical understanding of transition metal complexes, one has to realize that BDE values or bond lengths provide little insight into the intrinsic strength of a metal–ligand bond. The BDE is a reaction parameter that includes all changes during the dissociation both with regard to the reactant(s) and the product(s). Accordingly, it includes any (de)stabilization effect of the products to be formed. The magnitude of the BDE is determined by the energy needed for bond breaking, but also contains energy contributions due to rehybridization and electron density reorganization in the dissociation fragments, spin decoupling and recoupling energies, energy effects resulting from avoided crossings (in the case of diatomics) along the reaction path, Jahn–Teller or pseudo Jahn–Teller effects, conjugation possibilities in the fragments, etc. Although chemists tend to assume that the BDE directly reflects the energy and thereby the intrinsic strength of the bond to be broken, it cannot do this as it is strongly affected in non-predictable ways by the changes in the energies of the dissociation fragments. Often it cannot even be used in a qualitative manner as a bond

Computational and Theoretical Chemistry Group (CATCO), Department of Chemistry, Southern Methodist University, 3215 Daniel Ave, Dallas, Texas 75275-0314, USA. E-mail: dcremer@smu.edu

strength descriptor, so that the use of BDEs has led in many cases to a misjudgment of bond strength.^{16–21}

To obtain the intrinsic strength of a bond, the process of bond dissociation must be converted into a hypothetical process in which bond breaking is faster than the movement of the atoms in the fragments (10^{-15} s) but also faster than that of the fragment electrons (10^{-18} s) so that the electron density distribution of the fragments is frozen in the form of the original reactant and rehybridization effects, electron density relaxation effects due to conjugation, hyperconjugation, special 3-electron delocalization effects, *etc.* do not take place. Especially, the geometry of the fragments is frozen in that of the original molecule. Such a hypothetical process would lead to a much higher BDE value, which, contrary to the measured BDE values, could exactly reflect the intrinsic strength of a bond and therefore has been called the intrinsic BDE (IBDE, see Fig. 1) by Cremer and co-workers.²²

Although IBDEs cannot be measured, their introduction as a model quantity does lead to an alternative approach to the determination of the intrinsic strength of a bond. The BDE and IBDE are reactions or dynamic parameters corresponding to an infinitely large increase of the length of the bond to be broken. A finite increase of the bond distance during a molecular stretching vibration gets much closer to the ideal situation of a bond strength measurement without any change in the electronic structure of a molecule. For this purpose, the properties of a bond stretching vibration must be used to assess quantities, which (in)directly lead to the intrinsic strength of the bond under consideration. The stretching frequency is suited for this purpose only in a limited way as it depends on the masses of the vibrating bond atoms, which excludes a direct comparison of the bonds of isotopomers or in general bonds between atoms with different masses. Of

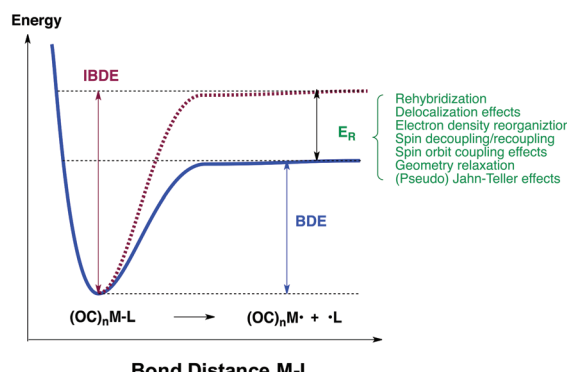
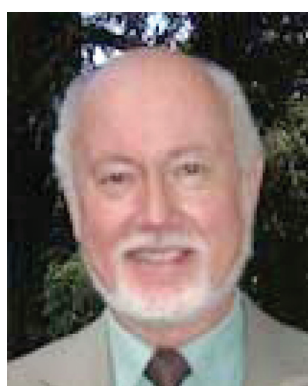


Fig. 1 Difference between the bond dissociation energy (BDE; blue) and the intrinsic bond dissociation energy (IBDE; dashed red line).

course, if the same type of bond is compared in different molecules (as for the TEP) a useful comparison in terms of stretching frequencies might result.

Better suited is the associated stretching force constant as it does not depend on the masses of the vibrating atoms and accordingly, directly relates to the electronic structure and intrinsic strength of a bond. In this connection, it is noteworthy to remember the definition of the stretching force constant (as well as of any other force constant relating to bending, internal rotation or torsion, ring puckering or ring deformation, *etc.*) as a second order response property being related to the second derivative of the energy with regard to the internal coordinate bond length. A second derivative of the energy reflects the rate of change in the energy for an infinitesimal change in the molecular geometry (*i.e.* the bond length). In other words, the stretching force constants gives the curvature of the potential energy surface (PES) in the direc-



Dieter Cremer

USA. He became Heisenberg Professor (Köln, 1983) and Full Professor at Göteborg University, Sweden (1990). His research ranges from the development of state-of-the-art relativistic methods to the study of chemical bonding. He has published more than 370 peer-reviewed research articles and presented his research at nearly 150 international conferences.



Elfi Kraka

Dr. Elfi Kraka is Professor and Chair of the Department of Chemistry at Southern Methodist University, Dallas, Texas, USA. She received her Dr. rer. nat. in Theoretical Chemistry at the University of Cologne, Germany (1985) with summa cum laude. Her recent research focuses on the study of chemical reactions with the “Unified Reaction Valley Approach” (URVA) and the computer-assisted drug design. She has published more than 165 peer-refereed articles and presented her research at about 80 international conferences. She is a member of the Scientific Board of the World Association of Theoretical and Computational Chemists (WATOC) and a member of the Editorial Boards of the Journal of Computational Chemistry and the International Journal of Quantum Chemistry.

tion of the infinitesimal change of bond length considered. This implies that the force constant measures a response of the electronic structure of the molecule without changing its electron density exactly as it is required by the IBDE measuring the intrinsic strength of the bond.²³

2. Development of ligand electronic parameters: the Tolman electronic parameter

Experimentalists have used vibrational properties to describe bonding in transition metal catalysts for a long time^{24–50} despite the fact that the rationalization of the use of vibrational properties was never derived on a physically or chemically sound basis. Vibrational force constants, although independent of the masses, turned out to be dependent of the coordinates used to describe a molecule, which made spectroscopists shy away from them^{51–55} and instead focused on vibrational frequencies, which were directly available from experiment. In the case of the transition metal complexes, M–L frequencies appear, because of the relatively large mass of M, in the far infrared or at least in a region difficult to analyze because bending and other framework frequencies are also found in this region. Therefore, the idea of a spectator ligand came up that had a high stretching frequency well-separated from all other frequencies and therefore easy to measure. The bond of the spectator ligand, and thereby its stretching frequency, had to be sensitive to the strength of the M–L bond or to electronic changes in connection with ligand replacements. Clearly, the spectator ligand had to be common to most transition metal complexes.

This idea was realized in several investigations in the 60s where, as suitable spectator and sensor ligands, nitriles, isonitriles, nitrosyl and carbonyl groups were tested. The CN, NC, NO⁺, or CO stretching frequency are sensitive with regard to the electronic configuration of a transition metal complex and a given M–L bond so that a spectroscopic (indirect) description of the latter seemed to be possible. Strohmeier's work on chromium, vanadium, manganese, tungsten, and other complexes^{56,57} made a lead in the field of metal-ligand investigations with contributions from Fischer,⁵⁸ Horrocks,^{59,60} and Cotton;^{61–64} Strohmeier ordered transition metals according to their π -donor ability: Cr > W > Mo > Mn > Fe. Apart from this, a general agreement was achieved concerning the impact of the ligand (L) on the transition metal (M). L can act as a σ -donor and a π -acceptor according to which the electron density is changed at M. This change can be sensed by the spectator ligand, which provides indirect evidence on the nature of L and the M–L bond.

Tolman^{65–67} was the first to provide a quantitative measure for the M–L bond strength by limiting the investigation to tertiary phosphines ($L = PR_3$) interacting with a nickel-tricarbonyl rest where the three CO ligands take the role of a spectator group measuring the interaction of L with Ni. The TEP

(Tolman Electronic Parameter) is based on the A_1 -symmetrical CO stretching frequency of a nickel tricarbonyl phosphine complex where Tolman established the relationship

$$\text{TEP} = \omega(\text{CO}, \text{Ni}, A_1) = 2056.1 + p_L \quad (1)$$

where PR_3 with $R = t\text{-Bu}$ was chosen as a suitable reference so that $p_L = 0$ and $\omega(\text{CO}, A_1) = 2056.1 \text{ cm}^{-1}$ results. Tolman considered $P(t\text{-Bu})_3$ as the most basic phosphine because of its strong σ -donor and absent π -acceptor ability. This leads to an increase of the electron density at Ni, which is transferred via the d-orbitals into the antibonding $\pi^*(\text{CO})$ orbitals (Fig. 2a or b). The CO bond length is increased and the A_1 -symmetrical CO stretching mode decreased to the value of 2056.1 cm^{-1} . Any other, less basic phosphine leads to a lower electron density at Ni and thereby a higher CO stretching frequency $\omega(L)$ and the ligand-specific increment $p_L = \omega(L) - 2056.1$. In this way, the basicity of phosphine ligands could be quantified by simply measuring the vibrational spectra (infrared or Raman) of the corresponding phosphine–nickel–tricarbonyl.

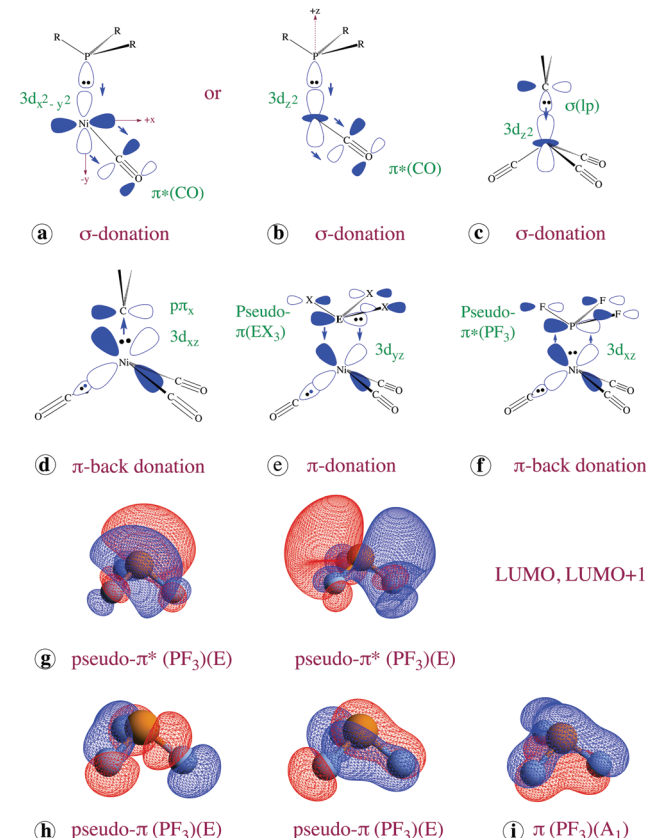


Fig. 2 Interactions between ligand (L) and the $\text{Ni}(\text{CO})_3$ group: (a, b) two different σ -donation modes from the lone-pair orbital (lp) of a phosphine to a $3d(\text{Ni})$ orbital that transfers density to the $\pi^*(\text{CO})$ orbital; (c, d) σ -donation of, and π -back donation to a carbene; (e) π -donation from an occupied pseudo- π orbital of EX_3 ($E: \text{As, Sb, Bi}; X: \text{methyl}$) to an empty $3d(\text{Ni})$ -orbital; (f) π -back-donation to the pseudo- π^* orbital of PF_3 ; (g) E -symmetrical pseudo- π^* orbitals of PF_3 with partly π - and partly σ -character; (h) E -symmetrical pseudo- π orbitals of PF_3 ; (i) the A_1 -symmetrical $\pi(\text{PF}_3)$ -orbital is clearly different from the pseudo- π orbitals.

Since the A_1 -symmetrical CO stretching frequency is separated from the metal, carbon stretching and bending frequencies, it can be easily detected and measured. Furthermore, this is the basis of Tolman's assumption that the CO-stretching frequencies are local, *i.e.* they do not couple with any of the other vibrational modes and therefore the TEP can be directly used as an electronic parameter, which does not depend on the technical details of the measurement.

Tolman's choice of reference was originally meant to obtain just positive p_L values, but since then the *t*-Bu reference has turned out to be useful just for phosphines as Arduengo carbenes, NHCs,^{68–70} are stronger σ -donors so that a TEP < 2056.1 cm^{−1} and a negative p_L value results. The investigation of literally hundreds of transition metal carbonyl complexes has tested the general applicability of the original Tolman concept. Otto and Roodt⁷¹ have fitted the CO frequencies measured by Strohmeier for *trans*-[Rh(CO)Cl₂] (Rh-Vaska) complexes with the CO frequencies of Tolman's nickel-tricarbonyl-phosphines and obtained a quadratic relationship, which suggests that, besides the σ -donor activity of the trialkylphosphines, for other ligands a second M–L bonding mechanism in the form of a strong π -acceptor ability becomes dominant. A series of 14 linear relationships between the TEP and the CO stretching frequencies of V, Cr, Mo, W, Mn, Fe, and Rh complexes has been published by Kühl:⁷²

$$\text{TEP} = a\omega(\text{CO}, \text{M}) + b \quad (2)$$

where each new type of a given transition metal complex (with the same transition metal M) required a different relationship and the correlation coefficient R^2 varied from 0.799 to 0.996. A significant data scattering suggested that for a given transition metal M and a given complex R_nM(CO)_mL (ligands R, L, and counters m and n vary) different M–L bonding mechanisms play a role that might be affected by the environment (solvent, crystal state, *etc.*). Fig. 3 gives the current use of the TEP in form of a TEP periodic table where the manifold of transition metal complexes for a given M can be retrieved from the literature given in the caption of Fig. 3.

The TEP Periodic Table										
Mg		Ti	V	Cr	Mn	Fe	Co	Ni	Cu	Zn
		Zr		Mo		Ru	Rh	Pd		
			W	Re	Os	Ir	Pt	Au		

Fig. 3 Use of the TEP throughout the periodic table. Experimentally derived TEPs have been discussed for Ni (blue: original scale)^{65–67,73–78} and correlated for complexes of those transition metals given in maroon by Kühl.⁷² For specific references, see Pd,^{79–83} Pt,^{82,84} Co,^{85,86} Rh,^{75,87–89} Ir,^{75,81,90–92} Fe,⁸⁷ Ru,^{93–98} Os,⁹⁹ Re,^{100–102} Mn,^{56,57,103} Cr,^{59,104–107} Mo,^{88,77,104} W,^{85,108} V,⁵⁷ Ti,^{109,110} Zr,¹¹¹ Mg,⁵⁷ Cu,¹¹² Au,^{113–115} Zn.⁸⁰

3. The adiabatic vibrational modes as the local equivalent of the normal modes

The normal vibrational modes in a molecule always couple. There are only a few examples for uncoupled, not delocalized, *i.e.* local vibrational modes. The bending vibration of the water molecule is such an example of a local vibration where the frequency is not contaminated by coupling contributions. Similarly, the Ni–P stretching vibration of (CO)₃Ni–PH₃ is by more than 99% uncoupled and local. In general, mode-mode coupling depends on the orientation of the mode vectors: local vibrational modes with orthogonal mode vectors do not couple. Also, the difference in masses can suppress coupling. For example, for the light–heavy–light arrangement of an acyclic three-atom molecule, the central atom can function as a “wall” thus largely suppressing mode-mode coupling.

There are two different coupling mechanisms between vibrational modes as a consequence of the fact that there is a kinetic and a potential contribution to the energy of a vibrational mode. The electronic coupling between modes is reflected by the off-diagonal elements of the force constant matrix. By diagonalizing the force constant matrix \mathbf{F}^q expressed in terms of internal coordinates q_n , electronic mode-mode coupling is eliminated.

There have been repeated attempts to derive from measured vibrational spectra force constants that determine the strength of a chemical bond. These attempts failed because the normal mode force constants depend on the internal coordinates chosen to describe the molecular geometry and, in addition, are still contaminated by kinematic mode-mode coupling. In the 60s, Decius⁵⁴ attempted to solve the force constant problem by using the inverse force constant matrix $\Gamma = (\mathbf{F}^q)^{-1}$ and introducing the compliance constants Γ_{nn} as bond strength descriptors. However, the relationship of the compliance constants to the normal or other vibrational modes was unclear. Hence, the compliance constants remained force constants without a vibrational mode and a frequency, which is a contradiction in itself as force constants are always associated with a dynamic process. Also a given Γ_{nn} had off-diagonal elements Γ_{mn} ($m \neq n$), the physical meaning of which was unclear. This led to justified criticism and questions about the usefulness of compliance constants.¹¹⁶ Why were just the Γ_{nn} terms used without considering the role of the Γ_{mn} when chemical bonds were described? What is the physical meaning of the compliance constants of redundant internal coordinates? Answers to these questions were provided by Cremer and co-workers^{117–119} who derived the equations for the local vibrational modes in form of the local equivalent of the Wilson equation for vibrational spectroscopy.¹²⁰ They showed that the compliance constants are model quantities and thereby superfluous as they have to be replaced by the physically well-based properties of the local vibrational modes.

Kinematic coupling or mass coupling leads to mode-mode coupling even then when the electronic coupling contribution

is eliminated by determining the normal vibrational modes. In 1998, Konkoli and Cremer^{117,121} determined for the first time local vibrational modes directly from normal vibrational modes by solving the mass-decoupled Euler–Lagrange equations. Each local mode is associated with an internal coordinate q_n ($n = 1, \dots, N_{\text{vib}}$ with $N_{\text{vib}} = 3N - \Sigma$; N : number of atoms; Σ : number of translations and rotations), which drives the local mode.¹¹⁷ Konkoli and Cremer also demonstrated that each normal vibrational mode can be characterized in terms of local vibrational modes, where their Characterization of Normal Mode (CNM) method is superior to the potential energy distribution analysis.^{119,121} Cremer and co-workers developed a way of calculating from a complete set of $3N - \Sigma$ measured fundamental frequencies the corresponding local mode frequencies.¹¹⁸ In this way, one can distinguish between calculated harmonic local mode frequencies (force constants) and experimentally-based local mode frequencies (force constants), which differ by anharmonicity effects.^{122,123} Zou and co-workers¹²⁴ proved that the reciprocal of the compliance constant of Decius is identical with the local force constant of Konkoli and Cremer so that for the first time the physical meaning of the compliance constants became obvious. Zou and co-workers proved also that the local vibrational modes of Konkoli and Cremer are the only modes, which directly relate to the normal vibrational modes.¹²⁴

Konkoli and Cremer developed the leading parameter principle,¹¹⁷ which says that for any internal, symmetry, curvilinear, etc. coordinate a local mode can be defined. This mode is independent of all other internal coordinates used to describe the geometry of a molecule, which means that it is also independent of using redundant or non-redundant coordinate sets. The number of local vibrational modes can be larger than N_{vib} and therefore it is important to determine those local modes, which are essential for the reproduction of the normal modes. They can be determined with the help of an Adiabatic Connection Scheme (ACS), which relates local vibrational frequencies to normal vibrational frequencies by increasing the scaling factor λ from zero (local frequencies) to 1 (normal frequencies). For a set of redundant internal coordinates and their associated local modes, all those frequencies converge to zero for $\lambda \rightarrow 1$, which do not contribute to the normal modes so that a set of N_{vib} dominant local modes remains.^{124,125} In this way, a 1 : 1 relationship between local (adiabatically relaxed) vibrational modes and normal vibrational modes is established.¹²⁴

A local stretching force constant associated with the bond length q_n is related to the second derivative of the molecular energy with regard to q_n , i.e. to the curvature of the Born–Oppenheimer potential energy surface (PES) $E(\mathbf{q})$ given in a specific direction defined by internal coordinate q_n of the molecule in question. For an increasing q_n , the bond length becomes the coordinate of bond dissociation. Zou and Cremer²³ demonstrated that by approximating the PES in this direction by a Morse potential and freezing the electron density during the dissociation process, the IBDE is directly related to the local stretching force constant, so that it is justi-

fied to consider the latter as a universal measure of the intrinsic strength of a bond. The adjective universal expresses the fact that the local stretching force constant of H_2 can be directly compared with that of the UO bond in UO_2 irrespective of the type of bonding, the positioning of the bond atoms in the periodic table, their electron shell structure (size of the core), electronegativity, or other properties.

A frequently asked question is whether the Konkoli–Cremer local modes can be measured. The successful measurement of local mode frequencies is well-documented in the literature. (i) McKean and co-workers^{126–128} solved the problem of obtaining local XH stretching frequencies and force constants by synthesizing isotopomers of a given molecule in such a way that all H atoms but the target-H were replaced by D. In the corresponding isotopomer, the XH stretching mode is largely decoupled from all other modes that involve now the much heavier D atoms. McKean and co-workers^{126–128} measured so-called isolated XH stretching frequencies, which reasonably approximate the local mode frequencies.¹²⁹

(ii) Henry¹³⁰ obtained local mode information for the CH stretching vibrations from overtone spectra. Intracavity dye laser photoacoustic spectroscopy uses sophisticated techniques to enhance the signal-to-noise ratio in the overtone spectra¹³⁰ so that overtones of XH stretching vibrations with $\Delta\nu = 5$ or 6 can be measured. For overtones with $\Delta\nu = 5, 6$, one observes mostly one band for each unique XH bond, even if there are several symmetry equivalent XH bonds in the molecule. For fundamental and lower overtone modes, there is always a splitting of the frequency into symmetry-paired frequencies (e.g., a symmetric and an antisymmetric mode frequency of two symmetry equivalent XH stretching modes), but this splitting virtually disappears for overtones with $\Delta\nu \geq 5$. In general, the different linear combinations of symmetry equivalent XH stretchings become effectively degenerate for the higher overtones so that these provide an insight into the local mode nature of the corresponding stretching mode. Kraka and co-workers¹¹⁹ correlated the measured frequencies for the fifth overtone of CH stretchings of alkanes, alkenes, and aromatic molecules^{131–133} with the corresponding calculated harmonic local modes and found a linear relationship ($R^2 = 0.99$) between these quantities thus confirming the local mode nature of Henry's overtone local modes.¹³⁰

(iii) The water bending mode and other examples such as the Ni–P stretching mode and PH_3 torsional mode (see below) seem to be local modes due to a favorable light–heavy–light combinations of atom masses and/or an orthogonal arrangement of the mode vectors. This happens frequently. However, for the detection of these modes, one needs the Konkoli–Cremer CNM method.¹²¹

Before discussing the basic equations of the local mode theory, it is useful to point out that the term local mode has been used by different authors in different ways. (i) In the Konkoli–Cremer method, the local vibrational modes are the unique and only equivalents of the normal modes that are obtained using the Wilson equation as the basic equation of vibrational spectroscopy. The Konkoli–Cremer local modes are

related to the isolated modes of McKean,¹²⁶ which represent good approximations of the former.

(ii) Henry and co-workers^{130,134–137} used the term local modes in connection with local mode (an)harmonic oscillator models to describe the overtones of XH stretching modes. Therefore, microwave spectroscopists and other experimentalists refer to local modes in connection with overtone spectroscopy.

(iii) Reiher and co-workers^{138–140} calculate unitarily transformed normal modes associated with a given band in the vibrational spectrum of a polymer where the criteria for the transformation are inspired by those applied for the localization of molecular orbitals. The authors speak in this case of local vibrational modes because the modes are localized in just a few units of a polymer. These so-called localized modes are still delocalized within the polymer units.

(iv) In solid state physics, the vibrational modes of an impurity in a solid material are called local modes.^{141,142}

4. Theory of local vibrational modes

The Wilson equation of vibrational spectroscopy is given by eqn (3):^{120,143,144}

$$\mathbf{F}^x \tilde{\mathbf{L}} = \mathbf{M} \tilde{\mathbf{L}} \Lambda \quad (3)$$

where \mathbf{F}^x is the force constant matrix expressed in Cartesian coordinates x_i ($i = 1, \dots, 3N$), \mathbf{M} the mass matrix, matrix $\tilde{\mathbf{L}}$ collects the vibrational eigenvectors $\tilde{\mathbf{l}}_\mu$ in its columns, and Λ is a diagonal matrix with the eigenvalues λ_μ , which lead to the (harmonic) vibrational frequencies ω_μ according to $\lambda_\mu = 4\pi^2 c^2 \omega_\mu^2$. In eqn (3), the number of vibrational modes is given by N_{vib} , i.e. Σ translational and rotational motions of the molecule are already eliminated. The tilde above a vector or matrix symbol indicates mass weighting. By diagonalizing the force constant matrix according to $\tilde{\mathbf{L}}^\dagger \mathbf{F}^x \tilde{\mathbf{L}} = \Lambda$ the normal mode eigenvectors and eigenvalues are obtained.

Usually, the normal mode vectors $\tilde{\mathbf{l}}_\mu$ are re-normalized according to $\mathbf{L} = \tilde{\mathbf{L}}(\mathbf{M}^R)^{1/2}$ where the elements of the mass matrix \mathbf{M}^R are given by $m_\mu^R = (\tilde{\mathbf{l}}_\mu^\dagger \tilde{\mathbf{l}}_\mu)^{-1}$ and represent the reduced mass of mode μ . eqn (3) can be written in different ways. For example, if one leaves out mass-weighting as in

$$\mathbf{F}^x \mathbf{L} = \mathbf{M} \Lambda \quad (4)$$

one gets $\mathbf{L}^\dagger \mathbf{F}^x \mathbf{L} = \mathbf{K}$ and $\mathbf{L}^\dagger \mathbf{M} \mathbf{L} = \mathbf{M}^R$, which define the diagonal normal force constant matrix \mathbf{K} and the reduced mass matrix \mathbf{M}^R , respectively.

One can express the molecular geometry in terms of internal coordinates q_n rather than Cartesian coordinates x_n and through this way, one gets the Wilson equation in a new form:¹²⁰

$$\mathbf{F}^q \tilde{\mathbf{D}} = \mathbf{G}^{-1} \tilde{\mathbf{D}} \Lambda \quad (5)$$

where $\tilde{\mathbf{D}}$ collects columnwise the normal mode vectors $\tilde{\mathbf{d}}_\mu$ ($\mu = 1, \dots, N_{\text{vib}}$), and matrix $\mathbf{G} = \mathbf{B} \mathbf{M}^{-1} \mathbf{B}^\dagger$ (Wilson matrix) gives the

kinetic energy in terms of internal coordinates.¹²⁰ The eigenvector matrix $\tilde{\mathbf{D}}$ has the property to diagonalize \mathbf{F}^q and to give $\tilde{\mathbf{D}}^\dagger \mathbf{F}^q \tilde{\mathbf{D}} = \Lambda$. If one does not mass-weight the matrix \mathbf{D} , and works with $\mathbf{bf}^q \mathbf{D} = \mathbf{G}^{-1} D \Lambda$, diagonalization leads to $\mathbf{D}^\dagger \mathbf{F}^q \mathbf{D} = \mathbf{K}$.

Properties of a local mode

The local mode vector \mathbf{a}_n associated with the internal coordinate q_n ($n = 1, \dots, N_{\text{para}}$ with N_{para} being the number of internal coordinates to specify the molecular geometry), which leads the mode, is given by¹¹⁷

$$\mathbf{a}_n = \frac{\mathbf{K}^{-1} \mathbf{d}_n^\dagger}{\mathbf{d}_n \mathbf{K}^{-1} \mathbf{d}_n^\dagger} \quad (6)$$

where the local mode is expressed in terms of normal coordinates Q_μ , \mathbf{K} is the diagonal normal mode force constant matrix (see above) and \mathbf{d}_n a row vector of the matrix \mathbf{D} . The local mode force constant k_n^a of mode n (superscript a denotes an adiabatically relaxed, *i.e.* local mode) is obtained with eqn (7):

$$k_n^a = \mathbf{a}_n^\dagger \mathbf{K} \mathbf{a}_n = (\mathbf{d}_n \mathbf{K}^{-1} \mathbf{d}_n^\dagger)^{-1} \quad (7)$$

Local mode force constants, contrary to normal mode force constants, have the advantage of being independent of the choice of the coordinates to describe the molecule in question.^{117,118} In recent work, Zou and co-workers proved that the compliance constants Γ_{nn} of Decius⁵⁴ are simply the reciprocal of the local mode force constants: $k_n^a = 1/\Gamma_{nn}$.^{124,125}

The reduced mass of the local mode \mathbf{a}_n is given by the diagonal element G_{nn} of the \mathbf{G} -matrix.¹¹⁷ Local mode force constant and mass are needed to determine the local mode frequency ω_n^a

$$(\omega_n^a)^2 = \frac{1}{4\pi^2 c^2} k_n^a G_{nn} \quad (8)$$

Apart from these properties, it is straightforward to determine the local mode infrared intensity or the Raman intensity.¹⁴⁵

Adiabatic connection scheme (ACS) relating local to normal mode frequencies.

With the help of the compliance matrix $\Gamma^q = (\mathbf{F}^q)^{-1}$, the vibrational eigenvalue eqn (5) can be expressed as¹²⁴

$$(\Gamma^q)^{-1} \tilde{\mathbf{D}} = \mathbf{G}^{-1} \tilde{\mathbf{D}} \Lambda \quad (9)$$

$$\mathbf{G} \tilde{\mathbf{R}} = \Gamma^q \tilde{\mathbf{R}} \Lambda \quad (10)$$

where a new eigenvector matrix $\tilde{\mathbf{R}}$ is given by

$$\tilde{\mathbf{R}} = (\Gamma^q)^{-1} \tilde{\mathbf{D}} = \mathbf{F}^q \tilde{\mathbf{D}} = (\tilde{\mathbf{D}}^{-1})^\dagger \mathbf{K} \quad (11)$$

Zou and co-workers partitioned the matrices Γ^q and \mathbf{G} into diagonal (Γ_d^q and \mathbf{G}_d) and off-diagonal parts (Γ_{od}^q and \mathbf{G}_{od}):¹²⁴

$$(\mathbf{G}_d + \lambda \mathbf{G}_{od}) \tilde{\mathbf{R}}_\lambda = (\Gamma_d^q + \lambda \Gamma_{od}^q) \tilde{\mathbf{R}}_\lambda \Lambda_\lambda \quad (12)$$

The off-diagonal parts can be successively switched on by increasing a scaling factor λ from zero to one so that the local modes given by the diagonal parts ($\lambda = 0$) are adiabatically con-

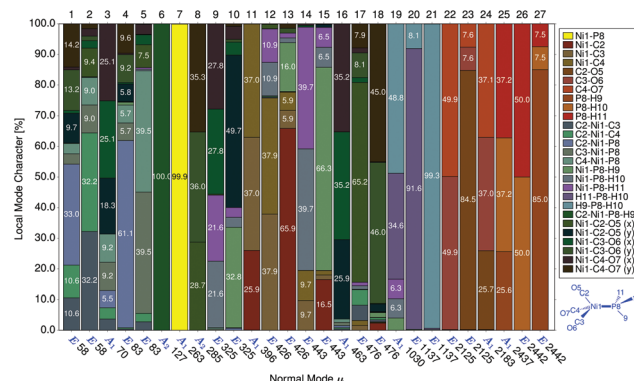


Fig. 4 Decomposition of the 27 normal vibrational modes of $(CO)_3Ni-PH_3$ into 27 local vibrational modes. Each of the 27 normal mode vectors d_μ is represented by a bar (mode number, symmetry, and calculated frequencies¹⁴⁶ are given at the top or bottom of each bar), which is decomposed in terms of 27 local mode vectors a_n . The local mode parameters are presented in the form of a color code (right side of diagram; for numbering of atoms, see diagram in the lower right corner.) Contributions larger than 5% are given within the partial bars representing a local mode.

verted into normal modes defined by $\lambda = 1$. Each λ defines a specific set of eigenvectors and eigenvalues collected in $\tilde{\mathbf{R}}_\lambda$ and Λ_λ , respectively, eqn (12) is the basis for the ACS.

As an example, the 27 normal modes of $(CO)_3Ni-PH_3$ are decomposed into 27 local modes and represented in a bar diagram where each bar corresponds to a normal mode displacement vector d_μ (Fig. 4). The local modes are color-coded (right side of Fig. 4). Their contribution to a given normal mode can be determined by the colors and the percentage numbers given in the bars, the length of which corresponds to 100%. In Fig. 5, the corresponding ACS is shown. For $\lambda = 1$, the normal mode frequencies ω_μ and the symmetries of the associated normal mode vectors are shown. Normal mode frequencies at $\lambda = 1$ are connected with local mode frequencies at $\lambda = 0$ by colored lines (red: A_1 ; blue: A_2 ; black: E symmetry) where the changes in the frequencies reflects kinematic coupling. The coupling of the CO stretching frequencies is significant and leads to a 53 cm^{-1} increase. This increase reveals that CO stretching is no longer local as all three CO stretching modes couple with each other. Hence, the TEP will be only reliable if the increase in the A_1 -mode frequency is constant for all $(CO)_3Ni-L$ complexes.

5. Deficiencies of ligand electronic parameters

Kalesky and co-workers¹⁴⁷ investigated the measured vibrational frequencies of the three transition metal carbonyls $Ni(CO)_4$ (T_d), $Fe(CO)_5$ (D_{3h}), and $Mo(CO)_6$ (O_h) that have 21, 27, and 33 vibrational modes. In Table 1, the experimental normal CO and MC stretching frequencies ω_μ are given together with their symmetries. Also listed are the corresponding CO and

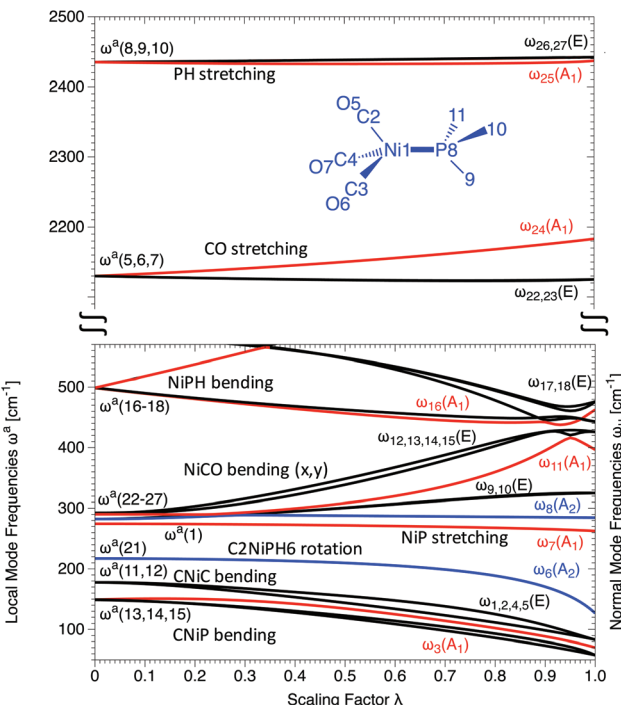


Fig. 5 Adiabatic connections scheme (ACS) of the 27 local vibrational modes of $(CO)_3Ni-PH_3$ as they are converted into 27 normal vibrational modes by changing the perturbation parameter λ from 0 to 1. The upper (CO stretching) and lower frequency ranges, respectively, are shown. The middle part from 600 to 2100 cm^{-1} of the ACS is not given. It contains local mode frequencies $\omega^a(19,20)$ (PH bending transforming into normal modes $\omega_{20,21}(E)$) and $\omega^a(2,3,4)$ (NiC stretching transforming into normal modes $\omega_{15,17,18}(E)$). The A_1 -symmetrical Ni–P stretching mode at 263 (red color) turns out to have a largely local mode character. For the decomposition of normal modes into local modes, compare with Fig. 4.

MC local stretching frequencies ω^a and associated stretching force constants k^a . The deviation of the ω_μ from the ω^a defines the coupling frequencies ω_{coup} and thereby the degree of mode-mode coupling. In the highly symmetrical transition metal carbonyls $Ni(CO)_4$, $Fe(CO)_5$, and $Mo(CO)_6$, Tolman would have expected zero-coupling for the $A_1(A'_1,A_{1g})$ -symmetrical CO stretching frequencies. Instead, CO, MC and CO, CMC-coupling leads to contamination of these frequencies by 69 , 74 , 24 , and 101 cm^{-1} (Table 1; for $Fe(CO)_5$, both the equatorial and axial A'_1 -symmetrical modes are considered). These are small deviations in view of the CO stretching frequencies of 2132 , 2121 , 2042 , and 2121 cm^{-1} (Table 1; see also Fig. 6). However, the TEP normally varies by far less than 100 cm^{-1} (variation of the TEP for phosphines: 31 cm^{-1})⁷² and therefore coupling frequencies of as much as 100 cm^{-1} are large. Problematic is also that for each of the three complexes compared in Table 1 a different coupling frequency is obtained, which makes the TEP highly erratic and thereby questionable.

The TEP and mode-mode coupling

A potential contamination of the CO stretching frequencies due to coupling was already considered by Crabtree and co-

Table 1 CO and MC experimental normal mode frequencies ω_μ and the corresponding local mode force constants k^a , local mode frequencies ω_n^a , and coupling frequencies ω_{coup} of $\text{Ni}(\text{CO})_4$, $\text{Fe}(\text{CO})_5$ and $\text{Mo}(\text{CO})_6$ ¹⁴⁷

Molecule, symmetry ^a	μ	Sym. ^b	$\omega_\mu [\text{cm}^{-1}]$	Parameter	$k^a [\text{mdyn \AA}^{-1}]$	$\omega^a [\text{cm}^{-1}]$	$\omega_{coup} [\text{cm}^{-1}]$
$\text{Ni}(\text{CO})_4$, T_d (21)	21	A_1	2132	CO	17.195	2063	69
	20	T_2	2058	CO	17.195	2063	-5
	17	T_2	459	NiC	1.900	570	-111
$\text{Fe}(\text{CO})_5$, D_{3h} (27)	9	A_1	371	NiC	1.900	570	-199
	27	A'_1	2121	CO	16.924	2047	74
	26	A'_1	2042	CO	16.456	2018	24
	25	A''_2	2034	CO	16.924	2047	-13
	24	E'	2013	CO	16.456	2019	-6
	22	E'	645	FeC	2.458	650	-5
	20	A''_2	619	FeC	2.510	657	-38
	14	A'_1	443	FeC	2.510	657	-214
$\text{Mo}(\text{CO})_6$, O_h (33)	11	A'_1	413	FeC	2.458	650	-237
	33	A_{1g}	2121	CO	16.482	2020	101
	32	E_g	2025	CO	16.482	2020	5
	30	T_{1u}	2003	CO	16.482	2020	-17
	18	A_{1g}	391	MoC	1.782	532	-141
	17	E_g	381	MoC	1.782	532	-151
	15	T_{1u}	367	MoC	1.782	532	-165

^a Number of normal modes in parentheses. ^b Sym. denotes the symmetry of the normal mode.

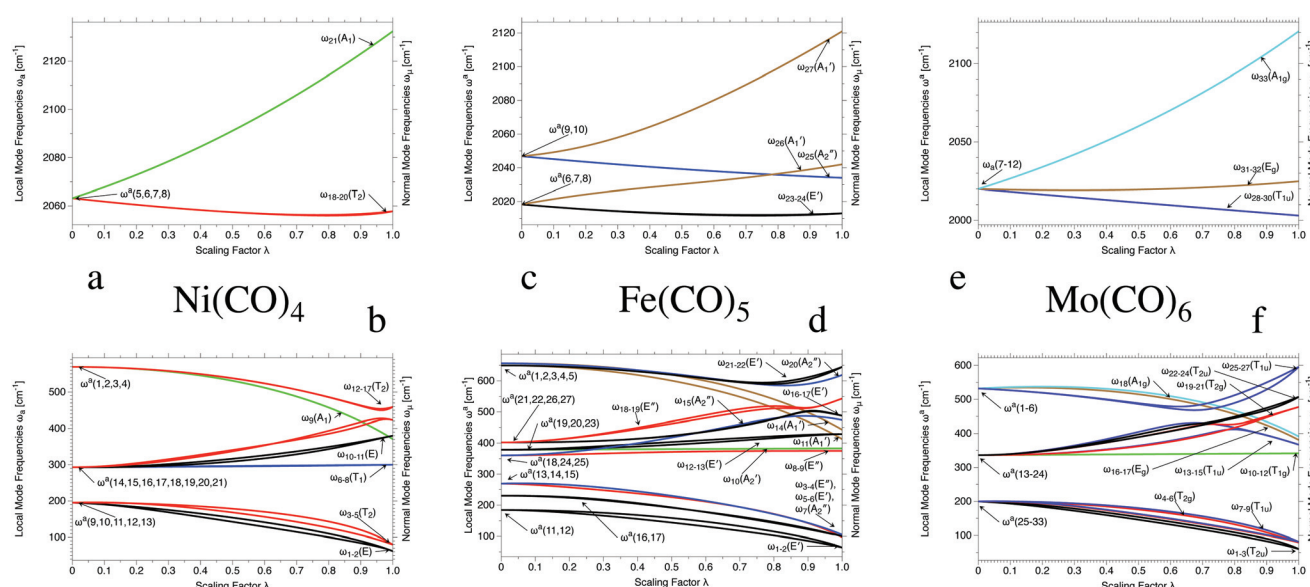


Fig. 6 ACS diagrams of (a, b) $\text{Ni}(\text{CO})_4$, (c, d) $\text{Fe}(\text{CO})_5$, and (e, f) $\text{Mo}(\text{CO})_6$. The upper diagrams show exclusively the CO stretching modes, whereas the lower diagrams show the M–C and other vibrational modes.¹⁴⁷

workers⁷³ who tried to computationally correct the CO stretching frequencies of 65 nickel-tricarbonyl complexes $\text{Ni}(\text{CO})_3\text{L}$. However, their attempt to eliminate mode-mode coupling by manipulating the Hessian of calculated energy second derivatives failed to remove the kinematic coupling between the CO stretching vibrations and other vibrations as was pointed out by Kalesky and co-workers.¹⁴⁷ These authors solved the coupling problem by utilizing the Konkoli–Cremer local vibrational modes and obtained for the first time decoupled CO stretching modes. Their TEP results are summarized in Fig. 7 for 65 nickel-tricarbonyl complexes $(\text{CO})_3\text{Ni-L}$.¹⁴⁷ If the TEP would be

without any coupling errors, data points would be found along the dashed line, which defines mode-decoupled, *i.e.* local TEP values. Instead data points (experimental: brown color; calculated: green color, Fig. 7) suggest more positive TEP values with decreasing local CO stretching frequency. Or in other words: a lower CO stretching frequency does not necessarily indicate a stronger Ni–CO π -back-bonding, but a larger mode-mode coupling. This holds for both measured and calculated TEP values.

This is confirmed when comparing coupling frequencies (the errors of the TEP values) directly with local CO stretching

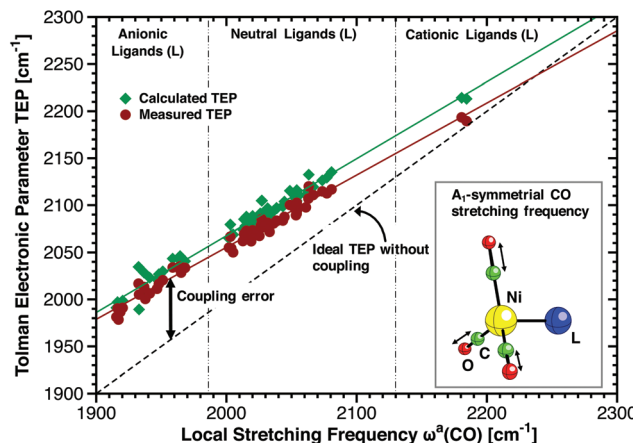


Fig. 7 Mode-mode coupling in nickel-tricarbonyl complexes leads to an erroneous TEP.¹⁴⁷

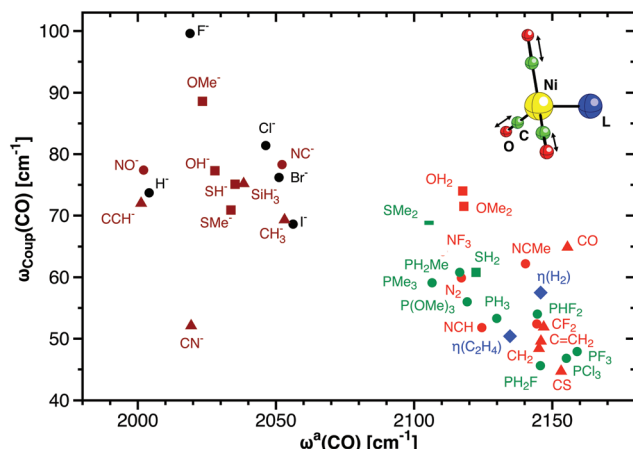


Fig. 8 CO Mode-mode coupling frequencies compared with the correct local CO stretching frequencies.¹⁴⁷

frequencies in Fig. 8. Anionic ligands with strong σ and/or π -donor capacity lead to the largest errors as Ni-CO π -back bonding is connected with a change in the Ni-C bond and an increase of Ni-C,CO coupling. This means that for neutral and anionic L, TEP errors of 40–100 cm^{-1} can be expected that make the use of the uncorrected TEP highly questionable. It seems that more electronegative ligands lead to higher TEP errors. Cationic ligands such as NO^+ or HC^+ give more reliable TEP values. As becomes obvious from an inspection of Fig. 8, there is no simple correction of TEP values.

Mode-mode coupling cannot be predicted without using local vibrational modes because it depends on the nature of the M-L bond, the mass of L, the symmetry of the complex, and its geometry. If for a given complex all N_{vib} vibrational frequencies are known, it is easy to determine the local CO stretching frequencies from measured normal mode frequencies as in the case of the three complexes of Table 1. For larger complexes, this becomes more and more difficult where however missing frequencies can be calculated using the har-

monic approximation and then adding anharmonicity corrections. Such a procedure would guarantee mode-coupling corrected TEP values. However, the following question has to be considered in such a case: does it make sense to use the TEP as an indirect descriptor of the M-L bond? If one is able to get the local CO stretching frequencies from measured frequencies, one can get, without any extra work, the local M-L stretching frequency. As frequencies depend on the reduced masses, one determines together with the local CO and M-L stretching frequencies ω^a also the corresponding local stretching force constants k^a , which can be directly compared. This makes it possible to assess the usefulness of Tolman's idea to describe M-L bonding utilizing the bond properties of the remote CO ligand.

Is there a relationship between the intrinsic strength of $\text{C}\equiv\text{O}$ and M-L bonding in transition metal carbonyl complexes?

This question was investigated by Setiawan and co-workers¹⁴⁶ who determined the local mode properties of 181 L-NiCO₃ complexes. In this connection, they compared the local Ni-L and CO stretching force constants, which should be closely related to justify the use of the TEP. The results of this investigation are summarized in Fig. 9 where the local stretching force constants k^a are compared. Clearly, there is no general relationship between $k^a(\text{CO})$ and $k^a(\text{NiL})$ contrary to Tolman's assumption. Subsets of data points belonging to a well-defined type of ligand may be connected by a linear relationship, but

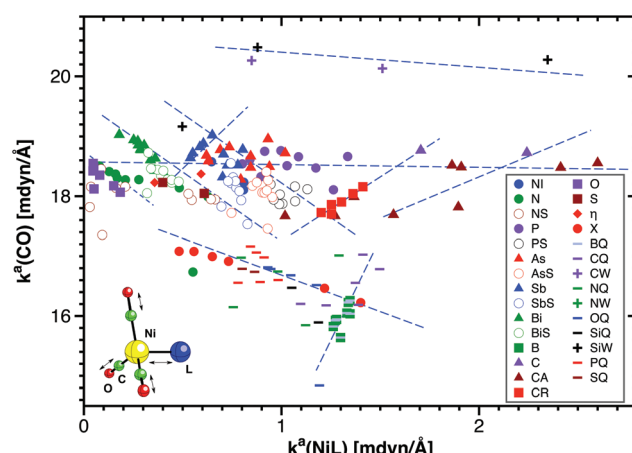


Fig. 9 There is no general relationship between the local TEP given by the local CO stretching force constant $k^a(\text{CO})$ and the intrinsic Ni-L bond strength given by the local Ni-L stretching force constant $k^a(\text{NiL})$.¹⁴⁶ Some possible relationships are indicated by dashed blue lines. Each group of ligands is indicated by a colored symbol; NI: nitrogen and cyano; N: amines; NS: amines with steric hindrance; P: phosphines; PS: phosphines with steric hindrance; As: arsines; AsS: arsines with steric hindrance; Sb: stilbines; SbS: stilbines with steric hindrance; Bi: bismuthines; BiS: bismuthines with steric hindrance; B: boron compounds; C: carbonyl, thiocarbonyl; CA: carbenes; CR: Arduengo carbenes; O: water and ethers; S: thioethers; η : haptic ligands; X: halogens; BQ: boron anions; CQ: carbanions; CW: carbocations; NQ: nitronium anions; NW: nitronium cations; OQ: hydroxides; SiQ: silicon anions; SiW: silicon cations; PQ: phosphonium anions; SQ: thiohydrides.

these relationships are different for different ligand types as is indicated in Fig. 9 by the different dashed lines. Some of these lines suggest an inverse relationship (a stronger Ni–L bond leads to a weaker CO bond), whereas others predict an increase of the CO bond strength with increasing NiL bond strength. In general, data point scattering is too large to derive any reliable mode of prediction. Even for the phosphines one has to distinguish between normal trialkyl phosphines (purple filled dots in Fig. 9), phosphines with electronegative substituents, and those with bulky substituents (sterically hindered phosphines, open green circles).

Since a general relationship between the intrinsic strength of the Ni–L bond and that of the CO bond is missing, the basic assumption of the TEP evaporates and the whole concept collapses. Hence, the TEP can be considered the result of an oversimplified bonding model. In view of the hundreds of TEP investigations, this is puzzling because adding more and more TEP investigations to the existing TEP literature does not make the deficiencies of Tolman's model vanish. The answer to this puzzle is simple. In most investigations the number of ligands considered was far smaller (often not more than 20) than the 181 ligands of the Setiawan investigation. If ligands have similar electronic properties (*e.g.*, the halogenides, the trialkylphosphines, *etc.*) a relationship might result, which for a larger set of ligands does not exist.

Tolman expected a reverse relationship between the M–L and CO bond strength. Any increase of the electron density at the metal atom leads to increased π -back donation, an increased population of the CO antibonding π -orbital, and a weakening of the CO bond that can be associated with a lower CO stretching frequency. According to Tolman, any increase of the electron density at M would indicate a stronger M–L bond due to stronger σ - or π -donation of L to M. This bonding model has to be strongly revised to capture the true electronic coupling between M–L and CO bond strength. Apart from this, there is no need to unravel this complicated relationship as the availability of $k^a(\text{NiL})$ provides a direct measure derived from experimental or calculated frequencies, which is far better than any indirect measure such as the TEP.

6. Application of the local vibrational modes: the metal–ligand electronic parameter MLEP

Tolman chose the A_1 -symmetrical CO stretching frequency because it can be easily measured in nearly all cases. Nowadays, accurate vibrational frequencies can be determined in the far-infrared utilizing Terahertz spectroscopy or depolarized Raman scattering. In view of the recent advances in Terahertz spectroscopy,^{148–150} far infrared absorptions down to 40 cm^{-1} can be measured, which includes the range where the measurement of the ML stretching frequencies becomes feasible. The local MC stretching frequencies of $\text{Ni}(\text{CO})_4$, $\text{Fe}(\text{CO})_5$, and $\text{Mo}(\text{CO})_6$ are 570, 650, 656, and 532 cm^{-1} and in each case

they are clearly separated from other local frequencies (Fig. 6: MC stretching frequencies are at the upper left part of (b), (d), and (f)). This is not the case for the corresponding normal mode frequencies, which by kinematic coupling mix with the MCO bending modes (Fig. 6). This is caused by avoided crossings of the T_2 -symmetrical modes 12–14 and 15–17 of $\text{Ni}(\text{CO})_4$, the A''_{2^-} (20 and 15) and T_2 -symmetrical modes (12–14 and 15–17) of $\text{Fe}(\text{CO})_5$, and the A''_{2^-} (20 and 15) and E' -symmetrical modes (21, 22 and 16, 17) of $\text{Mo}(\text{CO})_6$ in the range $0.90 < \lambda < 0.95$ (see Fig. 6). This makes a direct use of the normal mode frequencies for the characterization of the M–C bonds impossible.

One can apply far infrared spectroscopy in connection with the local mode analysis of Konkoli and Cremer and determine the local ML stretching force constants k^a utilizing measured frequencies^{118,122,123} and use the $k^a(\text{ML})$ values (Ni: 1.900; Fe: 2.458 (e), 2.510 (a); Mo: 1.782 mdyn Å⁻¹, Table 1) rather than the TEP as a reliable M–L describing electronic parameter (called by Setiawan and co-workers MLEP¹⁴⁶). In this way, it becomes obvious the Fe–C bonds are the stronger ones and that the axial bonds in $\text{Fe}(\text{CO})_5$ are slightly stronger than the equatorial ones, which is confirmed by the electron diffraction results in the gas phase (1.806 (ax) vs. 1.827 Å (eq.)),¹⁵¹ but not by the X-ray diffraction analysis.¹⁵²

Alternatively, one can calculate $k^a(\text{ML})$ values using accurate quantum chemical methods. Once the local ML stretching force constant $k^a(\text{ML})$ has been determined, one can simplify the comparison by deriving bond strength order (BSO) values n .^{18,21,153} The basis for this approach was laid by extending the Badger rule, which predicts for diatomic molecules a power relationship between stretching force constants and bond lengths.^{21,154} By using local stretching force constants and by replacing bond lengths by BSO values, the Badger relationship can also be applied to the bonds of polyatomic molecules. This could lead to a universal power relationship provided its form would be known. Instead the Badger relationship is used in an extended form, which says that different bonds between atoms of the same period found in polyatomic molecules can be described by one common power relationship relating local mode stretching force constants to BSO values as suitable bond strength descriptors. In this way, the range of different bonds investigated is reduced so that a larger accuracy results. An even better description in terms of BSO values n is guaranteed if just one type of bonding (*e.g.*, CO bonding) is compared. It is convenient to take the CO bond in methanol ($n = 1$) and that in formaldehyde ($n = 2$) as reference bonds to determine the constants a and b of the power relationship

$$n = a(k^a)^b \quad (13)$$

As a third condition, it is required that a force constant of zero leads to an n value of zero. Reference molecules and target molecules must be described in the same way to guarantee that reasonable BSO values result. For this reason, it is not useful to mix experimental and calculated frequencies for obtaining BSO values. Reliable quantum chemical methods

always lead to the same order of BSO values, *i.e.* the dependence on method and basis set is reduced. However, if the quantum chemical method in question is unable to describe the target and/or reference molecule, questionable BSO values will result.

There is always the problem of finding suitable reference bonds for non-covalent or transition metal bonds. In recent work, this problem was circumvented by using for two suitable reference molecules Mayer or Wiberg bond orders^{155,156} (*e.g.*, CuCH₃ and NiCH₂ as molecules being close to a M–C single and a M=C double bond) and defining the BSO relationship with the help of these reference values.¹⁴⁶

In Fig. 10, the relative BSO values of 181 NiL bonds are given as a power relationship of the calculated local stretching force constants $k^a(\text{NiL})$.¹⁴⁶ The majority of BSO values are relatively weak having $0 < n < 0.75$. The number of Ni–L single bonds ($0.75 < n < 1.25$) is limited to the group of carbenes whereas the interactions between ions (NO⁺, CH⁺, NS⁺, NSe⁺) and nickel lead to strong bonding with $n > 1.25$. The latter is the result of the fact that σ-donor and π-acceptor ability support each other (Fig. 2c and d).

Setiawan and co-workers¹⁴⁶ define the MLEP to be identical to the BSO values n being calculated with the same quantum chemical method and the same basis set. For another transition metal M, a different BSO relationship might be chosen. However, different power relationships can be easily merged by merging the reference bonds. In this way, the MLEP is an electronic parameter that does no longer depend on the masses of the atoms as the TEP, which cannot be merged with the results obtained for nitrosyl or nitrile ligands used as spectators as the reduced masses are different. Furthermore, the MLEP is a parameter that directly provides the intrinsic strength of M–L bond rather than that of another bond (TEP: CO bond), which is related to the M–L bond *via* a complicated bonding mechanism that cannot be necessarily predicted.

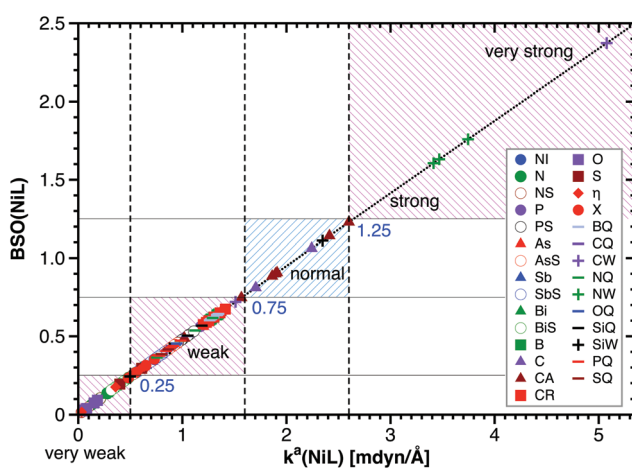


Fig. 10 The BSO value $n(\text{NiL})$ of Ni–L bonds given as a function of the local Ni–L stretching force constant $k^a(\text{NiL})$ using the equation $n = 0.480 \times (k^a)^{0.984}$. Regions of very weak, weak, normal, strong, and very strong Ni–L bonds are indicated by colored shading.¹⁴⁶

Intrinsic strength of nickel–phosphine bonding

In Fig. 11, the MLEP values of 20 phosphines are compared where both normal trialkyl phosphines, phosphines with electronegative substituents, and those with bulky substituents are included into the comparison. The MLEP values vary from 0.38 to 0.64 thus indicating that nickel–phosphine bonding is a relative soft bonding, which results primarily from the σ-donor property of the phosphine that increases the number of Ni valence electrons to 18.

As the H atoms in phosphine, PH₃, are more electronegative than P, the σ-donor capacity of the phosphine is reduced and an MLEP value of just 0.431 results. As shown by the bar diagram in Fig. 4, the Ni–P stretching mode (yellow bar) seems to not couple with any other vibrational mode, which is most likely a consequence of the mass ratios that represent a light (CO)-heavy (NiP)-light(H₃) situation. In so far, the A_1 -symmetrical Ni–P stretching mode frequency seems to be local, which implies that its associated stretching force constant can be directly used to determine the MLEP. Closer inspection of the ACS diagram in Fig. 5 reveals that kinematic coupling leads to a small change in the Ni–P stretching frequency, which has to be considered when determining the MLEP.

If the σ-donor capacity of a phosphine ligand is reduced by electronegative substituents, the MLEP should be reduced. However, for L = PF₃, one of the largest MLEP values (0.604 (ref. 146)) for phosphines is found. Setiawan and co-workers¹⁴⁶ determined the MLEP values of the nickel-ligand to increase in the order: PAt₃ < PI₃ < PH₃ < PBr₃ < PCl₃ < PF₃. This can be explained by considering that PF₃ has low-lying pseudo-π*(PF) orbitals that can obtain negative charge from the d(Ni) lone pair orbitals as is shown in Fig. 2f. The Ni–P bond is strengthened despite a reduced σ-donor ability of PF₃. Delocalization of a 3d(Ni) electron lone pair into a low-lying pseudo-π*(PX₃) orbital leads to an MLEP decrease with decreasing electronegativity of X from F (0.604) to At (0.386). This is in line with the energy increase of the pseudo-π*(PX₃) orbital (X = F, Cl, Br, I, At) and the reduced overlap between the 3d(Ni)-orbital and

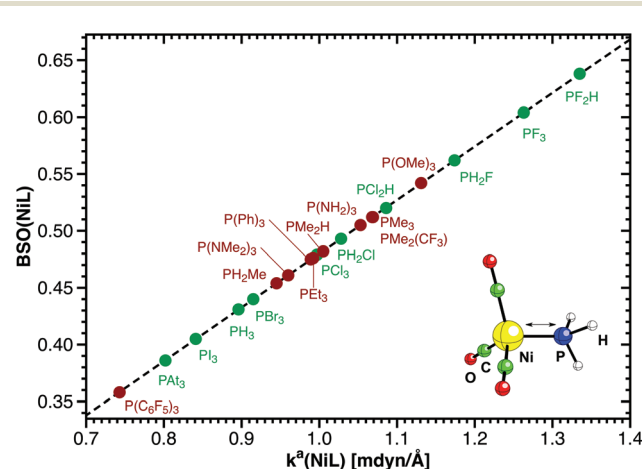


Fig. 11 Tolman's phosphines: the BSO value of Ni–P bonds given as a function of the local Ni–L stretching frequency.¹⁴⁶

the $3p\pi(P)$ -orbitals contributing to the pseudo- $\pi^*(PX_3)$ -orbital. The $3p\pi(P)$ -coefficient of the pseudo- $\pi^*(PX_3)$ orbital is large (see Fig. 2g) if the PX bond polarity is large (as a result of the orthogonality between pseudo- $\pi(PX_m)$ and pseudo- $\pi^*(PX_m)$ orbital), *i.e.* the larger electronegativity of X causes a larger overlap, stronger back-donation to the ligand and thereby a larger Ni–L bond strength. Hence, back donation to L must decrease in the series F, Cl, Br, H ~ I, At. One has also to consider a possible π -donor activity of the ligand involving an occupied pseudo- π orbital provided it has sufficient overlap and the orbital energy is in the range of that of the d(Ni) orbitals (Fig. 2e and h). This can certainly happen for E = As, Sb, Bi if the pnicogen substituents are alkyl groups. Apart from this, a 4e repulsive interaction with the occupied d(Ni) orbitals has also to be considered.

Since σ -bonding should increase from F(electronegativity $\chi = 4.10$ (ref. 157 and 158)) to Cl (2.83), Br (2.74), H (2.20) ~ I (2.21), and At (1.90), *i.e.* opposite to the observed trend, π -back donation to the trihalogenophosphine must be decisive overruling σ -donation. Other electronic effects such as steric bulk (increasing from PH_3 to PAt_3 and thereby weakening the Ni–L bond) or the relativistic contraction of the $5s(\text{I})$, $5p(\text{I})$ (or $6s(\text{At})$, $6p(\text{At})$) orbitals, which leads to a smaller $3p\pi(P)$ coefficient in the pseudo- $\pi^*(PX_3)$ orbital and reduced back-donation from Ni to L, also play a role. These effects cannot be revealed by the TEP that decreases from 2140 (PF_3) to 2135 (PCl_3), 2133 (PBr_3), 2129 (PI_3), and 2127 cm^{-1} (PAt_3) thus suggesting an increase rather than decrease of the Ni–L bond strength. The unusually strong Ni–P bond for the PF_2H ligand (0.638, Fig. 11) is the result of a favorable compromise between a limited weakening of the σ -donation effect (just two electronegative F substituents) and still strong π -back donation into the pseudo- $\pi^*(\text{PHF}_2)$ orbitals.

The change in the MLEP quantitatively reflects the intrinsic strength of the Ni–L bond as it results from electronic and/or steric effects. There is no need to include another electronic parameter that measures the steric bulk of a ligand as in the case of Tolman's cone angle θ .^{65,67} The MLEP includes all electronic effects that influence the intrinsic strength of the M–L bond and thereby also any steric influence. In the series PH_2Me (0.454) < PHMe_2 (0.482) < PMe_3 (0.512) ~ PMe_2CF_3 , σ -donation increases as a result of the donor-effect of the methyl group(s) whereas steric effects should play only a minor role. A phosphine with a CF_3 benefits from π -back donation thus balancing the reduction of σ -donation caused by the electronegative CF_3 -substituent.

Steric repulsion between L and the carbonyl ligands plays a role in the case of PET_3 (MLEP: 0.476; Fig. 11) and PPPh_3 (0.475). Even lower values of 0.461 for $\text{P}(\text{NMe}_2)_3$ and 0.358 for $\text{P}(\text{C}_6\text{F}_5)_3$ are due to steric interactions that weaken the Ni–P bond. These are documented by close contact between phosphine substituents and/or carbonyl atoms. $\text{P}(\text{C}_6\text{F}_5)_3$: repulsive interaction between the negatively charged, *o*-positioned F atoms at different phenyl groups; repulsion between F and O(C) atoms; $\text{P}(\text{NMe}_2)_3$: repulsion between positively charged H atoms of the methyl groups located at different amino groups and between the negatively charged N atoms. Tolman⁶⁷ saw

the necessity of complementing the CO stretching frequency by a cone angle that provides a qualitative measure for the steric effect of a ligand. However, a quantitative relationship between a cone angle and the strength of a metal–ligand bond is difficult to find and becomes superfluous as the MLEP based on the local Ni–L stretching force constant includes all electronic and steric factors influencing the ML bond strength.

As shown for the phosphines (Fig. 11), the MLEP can be easily determined for any other metal–ligand bond. Setiawan and co-workers¹⁴⁶ investigated the nickel-tricarbonyl-phosphines alongside the corresponding amines, arsines, stibines, and bismuthines. Apart from this, carbenes (especially Arduengo carbenes), dialkylethers and alkylthioethers, haptic ligands, halogens, boron ligands, cations and anions were studied. The authors showed that the MLEP, in contrast to the TEP, can easily be extended to any other M (including all those shown in the TEP periodic table of Fig. 1) and any other ligand L.

7. General use of the MLEP

With a few exceptions, the TEP has been limited to the description of transition metal carbonyl complexes. The MLEP can be determined for any metal or transition metal complex, whether it contains CO ligands or not. This is demonstrated in Fig. 12 for a collection of metal and transition metal complexes.¹⁷

Setiawan and co-workers¹⁷ investigated Pb–F and Pb–C single bonds in methylated lead molecules of the type $(\text{CH}_3)_n\text{Pb}(\text{n})\text{F}_{(2-n)}$ ($n = 0-2, 1-3$) and $(\text{CH}_3)_n\text{Pb}(\text{iv})\text{F}_{(4-n)}$ ($n = 0-4, 4-7$), Ti–P bonds in $\text{P}(\text{CH}_3)_3$, $\text{P}(\text{OC}_2\text{H}_5)_3$, and PF_3 adducts of open titanocene, $\text{Ti}(\eta^5\text{-2,4-C}_7\text{H}_{11})_2$ (8–11), and Cr–H or Cr– π bonds in chromium(II) hydride (12), chromocene (13), and cyclopentadienyl hydrides 14–17 (see Fig. 12). These authors used quantum chemical calculations to calculate the local M–L

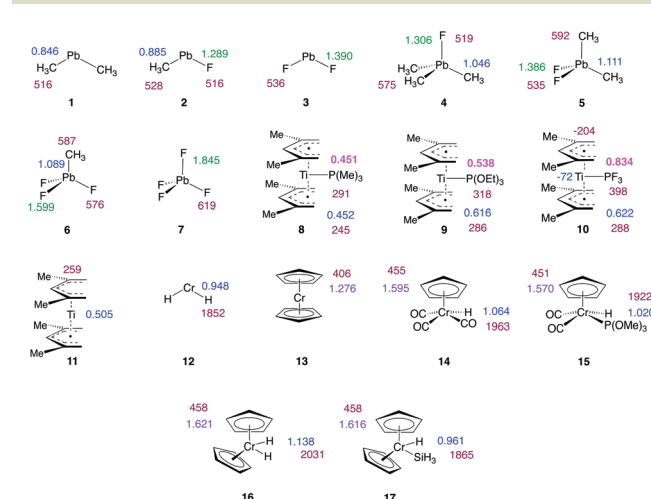


Fig. 12 Application of the MLEP to metal and transition metal complexes.¹⁷ MLEP values for Pb–C in blue, Pb–F in green, Ti–P in purple, Cr–H in blue, Ti– π in blue, and Cr– π in grape color. The corresponding local stretching frequencies are given in cm^{-1} and brown color.

stretching force constants, which makes it possible to determine the MLEP for each of the M–L bonds utilizing the power relationship given in Fig. 10. In Fig. 12, selected MLEP values are given for Pb–F (green) and Pb–C bonds (blue), which nicely reflect the increase in strength of the Pb–F bond with increasing fluorination and increasing polarity of the Pb–F bond. Other examples are the Ti–P bonds (purple), which increase with increasing electronegativity of the phosphine substituents, or the Cr–H bonds (blue), which depend on the electronic nature of the other ligands and the steric arrangement of the cyclopentadienyl anion ligand(s).

Finally, it is important to emphasize that the MLEP also provides a reliable measurement for the interaction of a metal atom with an aromatic ligand *via* the M···π stretching force constant. The latter is determined for the shortest distance between the metal atom and the π-system (Ti or Cr, grape color; Fig. 12). A strong interaction is determined for **16** where one has to consider that the Cu–C bond in CuCH₃ and the Ni=C bond in NiCH₂ are used as reference bonds.¹⁴⁶ Also shown in Fig. 12 are the local stretching frequencies (brown color) as they provide evidence for the normal mode frequency that is dominated by M–L stretching. All local frequency values are in the far infrared, which makes, in most cases, Terahertz spectroscopy a valuable source for the experimentally determined MLEP.

8. Conclusions

The idea of inventing a simple spectroscopic means, in the form of the CO-stretching frequency (TEP), to describe the metal–ligand bond is appealing, as it could be used to single out those ligands that can be easily replaced in the course of a catalytic reaction. However, there are two fundamental problems that make the TEP a questionable, largely misleading parameter. First, there is mode–mode coupling between CO and M–C stretching vibrations that leads to coupling errors, which are larger (20–200 cm⁻¹)¹⁴⁶ than the variation in the TEP. Second, the relationship between the M–L bond strength and TEP considered by Tolman as a key electronic feature of transition metal carbonyl complexes (CO)_nML_m is neither quantitatively nor qualitatively fulfilled for M–L because the electronic bonding mechanism is more complicated than described by Tolman⁶⁷ or in textbooks of inorganic chemistry.

This does not exclude that the basic assumptions of Tolman was and still is a valuable one. Vibrational spectroscopy, in the form of infrared, Raman, or the more modern Terahertz spectroscopy, provides sensitive tools to describe the electronic structure of any transition metal complex or any catalyst in general. There is only the necessity to convert measured normal mode frequencies into local mode frequencies utilizing the Konkoli–Cremer procedure and then deriving all other local mode properties needed, especially the local stretching force constants that reflect, in a universal way, the intrinsic strength of any bond.

The local stretching force constants $k^a(M-L)$ can be easily converted into relative bond strength orders (BSOs) which

provide a useful ordering of chemical bonds according to their strength. The MLEP is set equal to the BSO value and can, in this form, be easily compared from one M–L bond type to the other. This procedure can be carried out with measured or calculated data where, in the former case, a conversion from the normal mode into the local mode frequencies has to be carried out using suitable normal modes.¹¹⁸

Five different electronic effects have been identified, the interplay of which determines the strength of an M–L bond: (i) σ-donation of the ligand, (ii) steric interactions of the ligand with the M(CO)_n group, (iii) π-acceptor abilities of the ligand leading to delocalization of 3d(M) electrons, (iv) π-Donor abilities of the ligand leading to delocalization of the L electrons into empty M orbitals, and (v) scalar relativistic effects, of M or L being a “relativistic” element, which reduce the σ-donor capacity of the ligand besides also changing the π-acceptor and π-donor abilities.

Destabilizing steric interactions between L and an M(CO)_n group are directly determined by the MLEP and do not require a second geometric parameter such as a cone angle associated with L in the case of the TEP. Steric effects (exchange repulsion effects) of ligands such as triethyl, triphenyl, or triamino phosphines, amines, *etc.* are reflected by low MLEP values. If there is any need to separate them from other electronic effects, one can use the local C–M–L bending force constants, which, if measured relative to a suitable reference, provide a reliable quantitative measure of the exchange repulsion.

At this point, it is important to point out that the physical basis and the measurement of local mode properties is well-defined and does not involve any model of the chemical bond or molecular orbital theory. Accordingly, the MLEP, contrary to the TEP, is not a model quantity. However, the comparison of the MLEP with BDE values requires the IBDE as a model quantity, which so far can not be determined. The MLEP can be determined for any transition metal complex utilizing either experimental or computational techniques.

Currently, the MLEP is a static measure, which can be applied to a multitude of transition metal complexes such as Au-, Ru-, Rh-, Re-, or Ir-complexes to directly reflect the intrinsic strength of an M–L bond and any potential catalytic activity. There have already been attempts to also use the MLEP as a dynamic measure, *i.e.* measuring the activity of a catalyst during a catalyzed, chemical reaction.^{159,160}

Acknowledgements

This work was financially supported by the National Science Foundation, Grants CHE 1464906. We thank SMU for providing computational resources.

References

- 1 A. N. Desnoyer and J. A. Love, *Chem. Soc. Rev.*, 2017, **46**, 197–238.

- 2 G. Chelucci, *Coord. Chem. Rev.*, 2017, **31**, 1–36.
- 3 D. Li, X. Li and J. Gong, *Chem. Rev.*, 2016, **116**, 11529–11653.
- 4 A. Klein, A. Sandleben and N. Vogt, *Proc. Natl. Acad. Sci. U. S. A.*, 2016, **86**, 533–549.
- 5 W. Guan, G. Zeng, H. Kameo, Y. Nakao and S. Sakaki, *Chem. Rec.*, 2016, **16**, 2405–2425.
- 6 F. Julia-Hernandez, M. Gaydou, E. Serrano, M. van Gemmeren and R. Martin, *Top. Curr. Chem.*, 2016, **374**, 45–68.
- 7 R. L. Augustine, *Catal. Lett.*, 2016, **146**, 2393–2416.
- 8 *Contemporary Catalysis: Science, Technology, and Applications*, ed. C. J. K. Paul, Royal Society of Chemistry, London, Gld edn, 2017.
- 9 *Modern Developments in Catalysis*, ed. M. G. Davidson, C. Hardacre and N. J. Turner, World Scientific Publishing Europe Ltd, London, 2016.
- 10 S. Bhaduri and D. Mukesh, *Homogenous Catalysis*, Wiley, New York, 2014.
- 11 A. Zecchina and S. Califano, *The Development of Catalysis: A History of Key Processes and Personalities in Catalytic Science and Technology*, Wiley, New York, 2017.
- 12 *Applied Industrial Catalysis*, ed. J. C. S. Ruiz, Arcler Press LLC, New York, 2017.
- 13 R. Franke, D. Selent and A. Börner, *Chem. Rev.*, 2012, **112**, 5675–5732.
- 14 *Accounts of Chemical Research: Computational Catalysis for Organic Synthesis*, ed. G. E. Dean and J. Tantillo, ACS, 2016, vol. 46.
- 15 Y.-R. Luo, *Comprehensive Handbook of Chemical Bond Energies*, Taylor and Francis, Boca Raton, FL, 2007.
- 16 D. Setiawan, E. Kraka and D. Cremer, *J. Comput. Chem.*, 2016, **37**, 130–142.
- 17 D. Setiawan, E. Kraka and D. Cremer, *J. Phys. Chem. A*, 2015, **119**, 9541–9556.
- 18 E. Kraka and D. Cremer, *ChemPhysChem*, 2009, **10**, 686–698.
- 19 R. Kalescky, E. Kraka and D. Cremer, *Int. J. Quantum Chem.*, 2014, **114**, 1060–1072.
- 20 R. Kalescky, W. Zou, E. Kraka and D. Cremer, *J. Phys. Chem. A*, 2014, **118**, 1948–1963.
- 21 R. Kalescky, E. Kraka and D. Cremer, *J. Phys. Chem. A*, 2013, **117**, 8981–8995.
- 22 D. Cremer, A. Wu, A. Larsson and E. Kraka, *J. Mol. Model.*, 2000, **6**, 396.
- 23 W. Zou and D. Cremer, *Chem. – Eur. J.*, 2016, **22**, 4087–4089.
- 24 A. Kratzer, *Z. Phys.*, 1920, **3**, 289–307.
- 25 A. Kratzer, *Phys. Rev.*, 1925, **25**, 240–254.
- 26 R. Mecke, *Z. Phys.*, 1925, **32**, 823–834.
- 27 P. M. Morse, *Phys. Rev.*, 1929, **34**, 57–64.
- 28 R. M. Badger, *Phys. Rev.*, 1935, **48**, 284–285.
- 29 H. S. Allen and A. K. Longair, *Nature*, 1935, **135**, 764–764.
- 30 R. M. Badger, *J. Chem. Phys.*, 1935, **3**, 710–715.
- 31 M. L. Huggins, *J. Chem. Phys.*, 1935, **3**, 473–479.
- 32 M. L. Huggins, *J. Chem. Phys.*, 1936, **4**, 308–312.
- 33 G. B. B. M. Sutherland, *Proc. – Indian Acad. Sci.*, 1938, **8**, 341.
- 34 G. B. B. M. Sutherland, *J. Chem. Phys.*, 1940, **8**, 161–165.
- 35 C. H. D. Clark and K. R. Webb, *Trans. Faraday Soc.*, 1941, **37**, 293–298.
- 36 C. K. Wu and C. Yang, *J. Phys. Chem.*, 1944, **48**, 295–303.
- 37 J. W. Linnett, *Trans. Faraday Soc.*, 1945, **41**, 223–232.
- 38 W. Gordy, *J. Chem. Phys.*, 1946, **14**, 305–321.
- 39 C. K. Wu and S. C. Chao, *Phys. Rev.*, 1947, **71**, 118–121.
- 40 K. M. Guggenheim, *Discuss. Faraday Soc.*, 1950, **9**, 207–222.
- 41 G. Herzberg, *Spectra of Diatomic Molecules*, D. Van Nostand Co. Inc., Princeton, 2nd edn, 1950.
- 42 H. Siebert, *Z. Anorg. Allg. Chem.*, 1953, **273**, 170–182.
- 43 E. R. Lippincott and R. Schroeder, *J. Chem. Phys.*, 1955, **23**, 1131–1142.
- 44 H. O. Jenkins, *Trans. Faraday Soc.*, 1955, **51**, 1042–1051.
- 45 Y. P. Varshni, *J. Chem. Phys.*, 1958, **28**, 1078–1081.
- 46 Y. P. Varshni, *J. Chem. Phys.*, 1958, **28**, 1081–1089.
- 47 D. R. Hershbach and V. W. Laurie, *J. Chem. Phys.*, 1961, **35**, 458–463.
- 48 H. S. Johnston, *J. Am. Chem. Soc.*, 1964, **86**, 1643–1645.
- 49 J. A. Ladd, W. J. Orville-Thomas and B. C. Cox, *Spectrochim. Acta*, 1964, **20**, 1771–1780.
- 50 J. A. Ladd and W. J. Orville-Thomas, *Spectrochim. Acta*, 1966, **22**, 919–925.
- 51 W. J. Taylor and K. S. Pitzer, *J. Res. Nat. Bureau Stand.*, 1947, **38**, 1.
- 52 J. C. Decius, *J. Chem. Phys.*, 1953, **21**, 1121.
- 53 S. J. Cyvin and N. B. Slater, *Nature*, 1960, **188**, 485–485.
- 54 J. Decius, *J. Chem. Phys.*, 1963, **38**, 241.
- 55 S. J. Cyvin, *Molecular Vibrations and Mean Square Amplitudes*, Universitetsforlaget, 1971, pp. 68–73.
- 56 W. Strohmeier and J. Guttenberger, *Chem. Ber.*, 1964, **97**, 1871–1876.
- 57 W. Strohmeier and F. Müller, *Z. Naturforsch., B: Anorg. Chem. Org. Chem. Biochem. Biophys. Biol.*, 1967, **22**, 451–452.
- 58 R. Fischer, *Chem. Ber.*, 1960, **93**, 165–175.
- 59 W. D. Horrocks, Jr. and R. C. Taylor, *Inorg. Chem.*, 1963, **2**, 723–727.
- 60 G. R. V. Hecke and W. D. Horrocks, *Inorg. Chem.*, 1966, **5**, 1960–1968.
- 61 F. A. Cotton and F. Zingales, *Inorg. Chem.*, 1962, **1**, 145–147.
- 62 C. S. Kraihanzel and F. A. Cotton, *Inorg. Chem.*, 1963, **2**, 533–540.
- 63 F. A. Cotton, *Inorg. Chem.*, 1964, **3**, 702–711.
- 64 F. A. Cotton, A. Musco and G. Yagupsky, *Vib. Spectr. and Bonding in Metal Carbonyls*, 1967, **6**, 1357–1364.
- 65 C. A. Tolman, *J. Am. Chem. Soc.*, 1970, **92**, 2953–2956.
- 66 C. A. Tolman, *Chem. Soc. Rev.*, 1972, **1**, 337–353.
- 67 C. A. Tolman, *Chem. Rev.*, 1977, **77**, 313–348.
- 68 A. Arduengo III, R. Harlow and M. Kline, *J. Am. Chem. Soc.*, 1991, **113**, 361–363.
- 69 A. Arduengo III, R. Dias, R. Harlow and M. Kline, *J. Am. Chem. Soc.*, 1992, **114**, 5530–5534.

- 70 J. A. Anthony, *Acc. Chem. Res.*, 1999, **32**, 913–921.
- 71 A. Roodt, S. Otto and G. Steyl, *Coord. Chem. Rev.*, 2003, **245**, 121–137.
- 72 O. Kühl, *Coord. Chem. Rev.*, 2005, **249**, 693–704.
- 73 L. Perrin, E. Clot, O. Eisenstein, J. Loch and R. H. Crabtree, *Inorg. Chem.*, 2001, **40**, 5806–5811.
- 74 Z. Thammapongsy, I. M. Kha, J. W. Ziller and J. Y. Yang, *Dalton Trans.*, 2016, **45**, 9853–9859.
- 75 C. Mejuto, B. Royo, G. Guisado-Barrios and E. Peris, *Beilstein J. Org. Chem.*, 2015, **11**, 2584–2590.
- 76 M. A. Wünsche, P. Mehlmann, T. Witteler, F. Buß, P. Rathmann and F. Dielmann, *Angew. Chem., Int. Ed.*, 2015, **54**, 11857–11860.
- 77 M. B. Geeson, A. R. Jupp, J. E. McGrady and J. M. Goicoechea, *Chem. Commun.*, 2014, **50**, 12281–12284.
- 78 M. Tobisu, T. Morioka, A. Ohtsuki and N. Chatani, *Chem. Sci.*, 2015, **6**, 430–437.
- 79 T. Xu, F. Sha and H. Alper, *J. Am. Chem. Soc.*, 2016, **138**, 66629–66635.
- 80 B. Kim, N. Park, S. M. Lee, H. J. Kim and S. U. Son, *Polym. Chem.*, 2015, **6**, 7363–7367.
- 81 J. A. Mata, F. E. Hahn and E. Peris, *Chem. Sci.*, 2014, **5**, 1723–1732.
- 82 C. Makedonas and C. A. Mitsopoulou, *Eur. J. Inorg. Chem.*, 2007, **2007**, 4176–4189.
- 83 R. Crabtree, *J. Organomet. Chem.*, 2006, **691**, 3146–3150.
- 84 R. Romeo and G. Alibrandi, *Inorg. Chem.*, 1997, **36**, 4822–4830.
- 85 J. A. Denny and M. Y. Darensbourg, *Coord. Chem. Rev.*, 2016, **324**, 82–89.
- 86 P. N. Bungu and S. Otto, *Dalton Trans.*, 2011, **40**, 9238.
- 87 P. Ai, A. A. Danopoulos and P. Braunstein, *Dalton Trans.*, 2016, **45**, 4771–4779.
- 88 N. Xamonaki, A. Asimakopoulos, A. Balafas, M. Dasenaki, I. Choinopoulos, S. Coco, E. Simandiras and S. Koinis, *Inorg. Chem.*, 2016, **55**, 4771–4781.
- 89 K. C. Oliveira, S. N. Carvalhoa, M. F. Duarte, E. V. Gusevskaya, E. N. dos Santos, J. E. Karroumi, M. Gouygou and M. Urrutigoity, *Appl. Catal. A*, 2015, **497**, 10–16.
- 90 H. Valdes, M. Poyatos and E. Peris, *Inorg. Chem.*, 2015, **54**, 3654–3659.
- 91 B. J. A. van Weerdenburg, N. Eshuis, M. Tessari, F. P. J. T. Rutjes and M. C. Feiters, *Dalton Trans.*, 2015, **44**, 153–15390.
- 92 D. Tapu, Z. McCarty, L. Hutchinson, C. Ghattas, M. Chowdhury, J. Salerno and D. VanDerveer, *J. Organomet. Chem.*, 2014, **749**, 134–141.
- 93 I. Czerwinska, J. Far, C. Kune, C. Larriba-Andaluz, L. Delaude and E. De Pauw, *Dalton Trans.*, 2016, **45**, 6361–6370.
- 94 D. S. Weinberger and V. Lavallo, *Handbook of Metathesis: Catalyst Development and Mechanism*, Wiley-VCH Verlag GmbH, Berlin, 2015, pp. 87–95.
- 95 Y. Borguet, G. Zaragoza, A. Demonceau and L. Delaude, *Dalton Trans.*, 2015, **44**, 9744–9755.
- 96 C. T. Check, K. P. Jang, C. B. Schwamb, A. S. Wong, M. H. Wang and K. A. Scheidt, *Angew. Chem., Int. Ed.*, 2015, **54**, 4264–4268.
- 97 A. K. E. Gallien, D. Schaniel, T. Woiked and P. Klüfers, *Dalton Trans.*, 2014, **43**, 13278–13292.
- 98 C. D. Varnado, Jr., E. L. Rosen, M. S. Collins, V. M. Lynch and C. W. Bielawski, *Dalton Trans.*, 2013, **42**, 13251.
- 99 A. J. Poë and C. Moreno, *Organometallics*, 1999, **18**, 5518–5530.
- 100 A. Bhattacharya, J. P. Naskar, P. Saha, R. Ganguly, B. Saha, S. T. Choudhury and S. Chowdhury, *Inorg. Chim. Acta*, 2016, **447**, 168–175.
- 101 B. Schulze and U. S. Schubert, *Chem. Soc. Rev.*, 2014, **43**, 2522–2571.
- 102 R. M. Mampa, M. A. Fernandes and L. Carlton, *Organometallics*, 2014, **33**, 3283–3299.
- 103 W. Strohmeier and F.-J. Muller, *Chem. Ber.*, 1967, **100**, 2812.
- 104 I. A. Portnyagin and M. S. Nechaev, *J. Organomet. Chem.*, 2009, **694**, 3149–3153.
- 105 T. A. Magee, C. N. Matthews, T. S. Wang and J. Wotiz, *J. Am. Chem. Soc.*, 1961, **83**, 3200–3203.
- 106 A. M. Bond, S. W. Carr and R. Colton, *Organometallics*, 1984, **3**, 541–548.
- 107 S. Grim, D. Wheatland and W. McFarlane, *J. Am. Chem. Soc.*, 1967, **89**, 5573–5577.
- 108 L. Carlton, A. Emdin, A. Lemmerer and M. A. Fernandes, *Magn. Reson. Chem.*, 2008, **46**, S56–S62.
- 109 H. Lang, E. Meichel, T. Stein, C. Weber, J. Kralik, G. Rheinwald and H. Pritzkow, *J. Organomet. Chem.*, 2002, **664**, 150–160.
- 110 P. C. Möhring, N. Vlachakis, N. E. Grimmer and N. J. Coville, *J. Organomet. Chem.*, 1994, **483**, 159–166.
- 111 O. J. Metters, S. J. K. Forrest, H. A. Sparkes, I. Manners and D. F. Wass, *J. Am. Chem. Soc.*, 2016, **138**, 1994–2003.
- 112 R. Starosta, U. K. Komarnicka and M. Puchalska, *J. Lumin.*, 2014, **145**, 430–437.
- 113 G. Ciancaleoni, N. Scafuri, G. Bistoni, A. Macchioni, F. Tarantelli, D. Zuccaccia and L. Belpassi, *Inorg. Chem.*, 2014, **53**, 9907–9916.
- 114 G. Ciancaleoni, L. Biasiolo, G. Bistoni, A. Macchioni, F. Tarantelli, D. Zuccaccia and L. Belpassi, *Chem. – Eur. J.*, 2015, **21**, 2467–2473.
- 115 A. Collado, S. R. Patrick, D. Gasperini, S. Meiries and S. P. Nolan, *Beilstein J. Org. Chem.*, 2015, **11**, 1809–1814.
- 116 J. Baker and P. Pulay, *J. Am. Chem. Soc.*, 2006, **128**, 11324.
- 117 Z. Konkoli and D. Cremer, *Int. J. Quantum Chem.*, 1998, **67**, 1–9.
- 118 D. Cremer, J. A. Larsson and E. Kraka, *Theoretical and Computational Chemistry, Volume 5, Theoretical Organic Chemistry*, Elsevier, Amsterdam, 1998, pp. 259–327.
- 119 E. Kraka, J. A. Larsson and D. Cremer, *Computational Spectroscopy: Methods, Experiments and Applications*, John Wiley & Sons, New York, 2010, pp. 105–149.

- 120 E. B. Wilson, J. C. Decius and P. C. Cross, *Molecular Vibrations. The Theory of Infrared and Raman Vibrational Spectra*, McGraw-Hill, New York, 1955.
- 121 Z. Konkoli and D. Cremer, *Int. J. Quantum Chem.*, 1998, **67**, 29–40.
- 122 R. Kalescky, W. Zou, E. Kraka and D. Cremer, *Chem. Phys. Lett.*, 2012, **554**, 243–247.
- 123 R. Kalescky, E. Kraka and D. Cremer, *Mol. Phys.*, 2013, **111**, 1497–1510.
- 124 W. Zou, R. Kalescky, E. Kraka and D. Cremer, *J. Chem. Phys.*, 2012, **137**, 084114.
- 125 W. Zou, R. Kalescky, E. Kraka and D. Cremer, *J. Mol. Model.*, 2012, 1–13.
- 126 D. C. McKean, *Chem. Soc. Rev.*, 1978, **7**, 399.
- 127 J. L. Duncan, J. L. Harvie, D. C. McKean and C. Cradock, *J. Mol. Struct.*, 1986, **145**, 225.
- 128 W. F. Murphy, F. Zerbetto, J. L. Duncan and D. C. McKean, *J. Phys. Chem.*, 1993, **97**, 581.
- 129 J. Larsson and D. Cremer, *J. Mol. Struct.*, 1999, **485**, 385.
- 130 B. R. Henry, *Acc. Chem. Res.*, 1987, **20**, 429.
- 131 Y. Mizugai and M. Katayama, *Chem. Phys. Lett.*, 1980, **73**, 240–243.
- 132 J. S. Wong and C. B. Moore, *J. Chem. Phys.*, 1982, **73**, 603–615.
- 133 G. Sbrana and M. Muniz-Miranda, *J. Phys. Chem. A*, 1998, **102**, 7603–7608.
- 134 R. J. Hayward and B. R. Henry, *J. Mol. Spectrosc.*, 1975, **57**, 221–235.
- 135 H. G. Kjaergaard, H. Yu, B. J. Schattka, B. R. Henry and A. W. Tarr, *J. Chem. Phys.*, 1990, **93**, 6239–6248.
- 136 H. G. Kjaergaard, D. M. Turnbull and B. R. Henry, *J. Chem. Phys.*, 1993, **99**, 9438–9452.
- 137 Z. Rong, B. R. Henry, T. W. Robinson and H. G. Kjaergaard, *J. Phys. Chem. A*, 2005, **109**, 1033–1041.
- 138 C. R. Jacob, S. Luber and M. Reiher, *Chem. – Eur. J.*, 2009, **15**, 13491–13508.
- 139 C. R. Jacob and M. Reiher, *J. Chem. Phys.*, 2009, **130**, 084106.
- 140 V. Liegeois, C. R. Jacob, B. Champagne and M. Reiher, *J. Phys. Chem. A*, 2010, **114**, 7198–7212.
- 141 V. I. Sokolov, N. B. Grudzev and I. A. Farina, *Phys. Solid State*, 2003, **45**, 1638–1643.
- 142 M. J. L. Sangster and J. H. Harding, *J. Phys. C: Solid State Phys.*, 1986, **19**, 6153–6158.
- 143 L. A. Woodward, *Introduction to the Theory of Molecular Vibrations and Vibrational Spectroscopy*, Oxford University Press, Oxford, 1972.
- 144 S. Califano, *Vibrational States*, Wiley, London, 1976.
- 145 W. Zou and D. Cremer, *Theor. Chem. Acc.*, 2014, **133**, 1451.
- 146 D. Setiawan, R. Kalescky, E. Kraka and D. Cremer, *J. Inorg. Chem.*, 2016, **55**, 2332–2344.
- 147 R. Kalescky, E. Kraka and D. Cremer, *Inorg. Chem.*, 2014, **53**, 478–495.
- 148 A. I. McIntosh, B. Yang, S. M. Goldup, M. Watkinson and R. S. Donnan, *Chem. Soc. Rev.*, 2012, **41**, 2072–2082.
- 149 H. H. Mantsch and D. Naumann, *J. Mol. Struct.*, 2010, **964**, 1–4.
- 150 E. P. J. Parrott, Y. Sun and E. Pickwell-MacPherson, *J. Mol. Struct.*, 2011, **1006**, 66–76.
- 151 B. Beagley and D. G. Schmidling, *J. Mol. Struct.*, 1974, **22**, 466.
- 152 D. Braga, F. Grepioni and A. Orpen, *Organometallics*, 1993, **12**, 1481.
- 153 M. Freindorf, E. Kraka and D. Cremer, *Int. J. Quantum Chem.*, 2012, **112**, 3174–3187.
- 154 R. M. Badger, *J. Chem. Phys.*, 1934, **2**, 128–131.
- 155 K. Wiberg, *Tetrahedron*, 1968, **24**, 1083–1096.
- 156 I. Mayer, *J. Comput. Chem.*, 2007, **28**, 204–221.
- 157 W. W. Porterfield, *Inorganic Chemistry, A Unified Approach*, Academic Press, San Diego, CA, 1993.
- 158 S. Anderson, *Introduction to Inorganic Chemistry*, University Science Books, Sausalito, CA, 2004.
- 159 W. Zou, T. Sexton, E. Kraka, M. Freindorf and D. Cremer, *J. Chem. Theory Comput.*, 2016, **12**, 650–663.
- 160 M. C. Reis, C. S. Lopez, E. Kraka, D. Cremer and O. N. Faza, *Inorg. Chem.*, 2016, **55**, 8636–8645.